Effects of Nonlinearity on the Atmospheric Flow Response to Low-Level Heating in a Uniform Flow

JONG-JIN BAIK

Department of Environmental Science and Engineering, Kwangju Institute of Science and Technology, Kwangju, Korea

HYE-YEONG CHUN

Department of Astronomy and Atmospheric Sciences, Yonsei University, Seoul, Korea

(Manuscript received 12 January 1995, in final form 28 December 1995)

ABSTRACT

Effects of nonlinearity on the stably stratified atmospheric response to prescribed low-level heating in a uniform flow are investigated through nondimensional numerical model experiments over a wide range of the nonlinearity factors of thermally induced finite-amplitude waves ($0 \leq \mu \leq 4$). The heating function is assumed to be uniform in the vertical from the surface to a nondimensional height of 2 and to be bell shaped in the horizontal.

As the nonlinearity factor becomes larger, the flow response is quite different from the linear response due to the larger nonlinear advective effect. A strong updraft cell gradually appears on the downstream side with an increasing nonlinearity factor. In the highly nonlinear regime ($\mu \geq 2.2$), alternating weaker downdraft and updraft cells behind the leading updraft cell are observed on the downstream side. These alternating cells experience periodic cycles with the processes of linear and nonlinear advection, intensification, weakening, formation, disappearing, and merging to the leading updraft cell. These processes are connected with the oscillatory behavior of the perturbation horizontal velocity through the mass continuity equation for the hydrostatic, incompressible flow. In the highly nonlinear regime, there exists the secondary maximum of the perturbation horizontal velocity at the surface, which during its downstream advection intensifies, causes the primary maximum of the perturbation horizontal velocity to diminish, and becomes a new primary maximum for an oscillation period. It is suggested that the repeated formation of the secondary maximum of the perturbation horizontal velocity and its becoming the primary maximum are responsible for the oscillatory processes and the steadiness of the maximum perturbation averaged for an oscillation period. As the nonlinearity factor increases, the oscillation period decreases.

1. Introduction

Theoretical aspects of the linear response of a stably stratified atmosphere to thermal forcing have been studied extensively because of its mathematical tractability and a broad range of applications to mesoscale circulation systems [see review papers by Lin and Stewart (1991) and Lin (1994)]. These applications include flow over heat islands (e.g., Olfe and Lee 1971; Baik 1992), orographically forced precipitating clouds (e.g., Fraser et al. 1973; Barcilon et al. 1980; Smith and Lin 1982), mesoscale moist convection (e.g., Thorpe et al. 1980; Raymond 1986; Lin and Chun 1991), internal gravity waves generated on an inversion (Lin and Goff 1988), and so on.

However, many mesoscale airflow systems observed in nature significantly deviate from the linear system, and it is indeed the nonlinear nature that makes airflow response to thermal forcing unexpectedly fascinating. Recently, in a study of the effects of diabatic cooling in a shear flow with a critical level, Lin and Chun (1991) proposed a nonlinearity factor of thermally induced waves. Baik (1992) applied this nonlinearity factor to the heat island problem using a numerical model in order to explain some dynamical aspects of precipitation enhancement observed on the downstream side of the heat island. Chun and Baik (1994) solved a steady-state, weakly nonlinear problem through perturbation expansion in a small value of the nonlinearity factor. They found that the main nonlinear effect is to produce a strong convergence region near the surface regardless of the specified forcing type—that is, heating or cooling. The next challenging theoretical step along this research line would be to consider a steady-state, fully nonlinear analytical problem. However, this problem appears to be extremely difficult, even though the Adomian decomposition method

Corresponding author address: Prof. Jong-Jin Baik, Department of Environmental Science and Engineering, Kwangju Institute of Science and Technology, 572 Sangam-dong, Kwangsan-ku, Kwangju 506-303, Korea.

provides hope for solving some nonlinear problems in a rapidly converging series form without resorting to weak nonlinearity (Adomian 1994).

In this paper, we extend our previous studies to investigate effects of nonlinearity on the atmospheric flow response to low-level heating using a time-dependent nondimensional numerical model. Numerical experiments with a wide range of the nonlinearity factors of thermally induced waves enable us to examine nonlinear effects. A simple flow system with a constant stability and a uniform basic-state flow is employed to delineate essential features of nonlinearity that are revealed in the thermally induced circulations. In section 2, a nondimensional model used in this study is described. In section 3, model results on the perturbation flow characteristics are presented and discussed. Summary and conclusions are given in section 4.

2. Nondimensional model

We consider a two-dimensional, hydrostatic, nonrotating, Boussinesq airflow system. The equations governing perturbations in a uniform basic-state horizontal wind with diabatic heating can be written as

$$\frac{\partial u}{\partial t} + U\frac{\partial u}{\partial x} + u\frac{\partial u}{\partial x} + w\frac{\partial u}{\partial z} = -\frac{\partial \pi}{\partial x} - \nu u, \quad (1)$$

$$\frac{\partial b}{\partial t} + U\frac{\partial b}{\partial x} + u\frac{\partial b}{\partial x} + w\frac{\partial b}{\partial z} + N^2 w = \frac{g}{c_p T_0} q - \nu b, \quad (2)$$

$$\frac{\partial u}{\partial x} + \frac{\partial w}{\partial z} = 0, \quad (3)$$

$$\frac{\partial \pi}{\partial z} = b, \quad (4)$$

where t is the time, x is the horizontal coordinate, z is the vertical coordinate, u is the perturbation wind velocity in the x direction, w is the perturbation wind velocity in the z direction, b is the perturbation buoyancy, π is the perturbation kinematic pressure, U is the basic-state wind velocity in the x direction ($U > 0$ in this study), ν is the coefficient of Rayleigh friction and Newtonian cooling, N is the Brunt–Väisälä frequency, g is the gravitational acceleration, c_p is the specific heat of air at constant pressure, and T_0 is a constant reference temperature. The diabatic heating q is specified as

$$q(x, z) = q_0 f(x) g(z), \quad (5)$$

$$f(x) = \frac{a_1^2}{x^2 + a_1^2} - \frac{a_1 a_2}{x^2 + a_2^2}, \quad (6)$$

$$g(z) = \begin{cases} 1 & \text{for} \quad 0 \le z \le d \\ 0 & \text{for} \quad z > d, \end{cases} \quad (7)$$

where q_0 is the amplitude of the heating function, a_1 (half-width of the bell-shaped function) and a_2 are constants ($a_1 < a_2$), and d is the heating top height (heating depth). The widespread cooling term [second term on the right-hand side of (6)] is included to avoid the net heating problem in a steady-state, inviscid flow system (Smith and Lin 1982).

We nondimensionalize the model variables as follows:

$$t = \left(\frac{L}{U}\right)\hat{t}$$

$$x = L\hat{x}, \quad a_1 = L\hat{a}_1, \quad a_2 = L\hat{a}_2$$

$$z = \left(\frac{U}{N}\right)\hat{z}, \quad d = \left(\frac{U}{N}\right)\hat{d}$$

$$u = \left(\frac{g q_0 L}{c_p T_0 N U}\right)\hat{u}$$

$$w = \left(\frac{g q_0}{c_p T_0 N^2}\right)\hat{w}$$

$$b = \left(\frac{g q_0 L}{c_p T_0 U}\right)\hat{b}$$

$$\pi = \left(\frac{g q_0 L}{c_p T_0 N}\right)\hat{\pi}$$

$$\nu = \left(\frac{U}{L}\right)\hat{\nu}$$

$$q = q_0 \hat{q}, \quad (8)$$

where L represents the horizontal length scale of the diabatic heating and the caret quantities are dimensionless. Applying the above scalings in (8) to (1)–(7) results in the following nondimensional equation set (with all the carets dropped hereafter):

$$\frac{\partial u}{\partial t} + \frac{\partial u}{\partial x} + \mu\left(u\frac{\partial u}{\partial x} + w\frac{\partial u}{\partial z}\right) = -\frac{\partial \pi}{\partial x} - \nu u, \quad (9)$$

$$\frac{\partial b}{\partial t} + \frac{\partial b}{\partial x} + w + \mu\left(u\frac{\partial b}{\partial x} + w\frac{\partial b}{\partial z}\right) = q - \nu b, \quad (10)$$

$$\frac{\partial u}{\partial x} + \frac{\partial w}{\partial z} = 0, \quad (11)$$

$$\frac{\partial \pi}{\partial z} = b, \quad (12)$$

$$q(x, z) = f(x) g(z), \quad (13)$$

$$f(x) = \frac{a_1^2}{x^2 + a_1^2} - \frac{a_1 a_2}{x^2 + a_2^2}, \quad (14)$$

$$g(z) = \begin{cases} 1 & \text{for} \quad 0 \le z \le d \\ 0 & \text{for} \quad z > d, \end{cases} \quad (15)$$

$$\mu = \frac{gq_0L}{c_pT_0NU^2}. \quad (16)$$

Note that the variables in (6) are in the dimensional form, while the variables in (14) are in the nondimensional form. The μ defined in (16) is called the nonlinearity factor of thermally induced finite-amplitude waves, which was first introduced by Lin and Chun (1991) in their study of the effects of diabatic cooling in a shear flow with a critical level. This nonlinearity factor can be interpreted as a scale ratio of the perturbation horizontal wind to the basic-state wind.

The nondimensional equations (9)–(12) are solved numerically using the finite-difference method. The fourth-order compact implicit scheme (Navon and Riphagen 1979) is employed for the first derivative terms with respect to x and the centered difference scheme for the first derivative terms with respect to z. The diffusion terms are time marched with the forward difference scheme and all the other terms with the leap-frog scheme. A lower boundary condition of $w = 0$ at $z = 0$ is imposed (flat surface). To minimize gravity wave reflection at the boundaries, the radiation condition at lateral boundaries proposed by Orlanski (1976) and the upper radiation condition proposed by Klemp and Durran (1983) are implemented in the model. The Asselin (1972) time filter is used to prevent the time separation of numerical solutions associated with the leap-frog scheme, and the space smoothing of the fourth-order diffusion type (Perkey 1976) is applied to reduce high-frequency numerical noise. The horizontal and vertical domain sizes are 10 and 12, respectively, with a horizontal grid spacing of 0.05 and a vertical grid spacing of 0.2 (201 × 61 grid points). The model is integrated up to $t = 8$ with a time interval of 0.00125. For all the model simulations, we set $\nu = 0.2$, $a_1 = 0.5$, $a_2 = 5a_1$, and $d = 2$, unless otherwise mentioned.

3. Results and discussion

To examine the effects of nonlinearity on the atmospheric flow response to low-level heating in a uniform basic-state flow, we performed numerical experiments with a wide range of the nonlinearity factors of thermally induced waves, ranging from $\mu = 0$ to 4 with a 0.2 increment (that is, $\mu = 0, 0.2, 0.4, \cdots, 3.8$, and 4).

Figure 1 shows the vertical velocity fields for the nonlinearity factors of 0.2, 0.6, 1, 2, 3, and 4 at a time step $t = 7$. As should be expected, when the nonlinearity factor is small (Figs. 1a and 1b), the flow response field is similar to that obtained analytically for a linear, steady-state, inviscid flow system (e.g., Baik 1992). This includes the successive bands of positive and negative vertical velocities with an upstream phase tilt, which implies an upward energy propagation, the downward motion on the upstream side of the heating, and the upward motion on the downstream side of the heating. These are typical characteristics that thermally induced gravity waves produce in the presence of a basic flow.

However, as shown in Figs. 1c–f, as the nonlinearity factor becomes larger, the flow response becomes quite different from the linear response because of the increasing nonlinear advective effect. In the case of $\mu = 1$, a strong updraft cell is distinctly observed on the downstream side. In each case of $\mu = 2$, 3, and 4, besides a leading strong updraft cell located on the downstream side, characteristically observed are the alternating weaker downdraft and updraft cells behind the leading updraft cell. These alternating cells are more pronounced in the cases of $\mu = 3$ and 4 than in the case of $\mu = 2$. Also, it is observed that the horizontal length scale of the leading updraft cells in the cases of $\mu = 2$, 3, and 4 is smaller than that in the case of $\mu = 1$ and the vertical length scale of the leading updraft cells in the formal three cases, which is about 2.5 times the heating depth ($d = 2$), is slightly larger than that in the latter case, which is about twice the heating depth. Figure 1 clearly demonstrates how the flow response regime drastically changes with increasing nonlinearity.

Irrespective of the chosen nonlinearity factors, all the vertical velocity fields in Fig. 1 exhibit a negative phase relationship between the heating and the induced vertical displacement in the vicinity of the heating center and the successive bands of positive and negative vertical velocities with an upstream phase tilt on the upstream side. In the cases with larger nonlinearity factors, the latter common feature is more identifiable when a denser contour interval is used as illustrated in Fig. 2 in the case of $\mu = 2$. In the linearized system, the curious negative phase relationship is directly related to the steadiness of the heating (Lin and Smith 1986; Bretherton 1988). This can be explained by either finding a solution for the vertical displacement at the origin of the heating in a view of the steady-state heat source as a train of heat pulses or an energy equation argument (Lin 1994).

Figure 1 shows that the leading updraft cell simulated with large nonlinearity factor appears to act as a steady forcing for the wave disturbance above it. Figures 1d and 2 show that the wave amplitude induced by the steady heating is small compared with that by the leading updraft cell. Since the structure of the wave disturbance induced by the forcing is characterized by the forcing structure as well as the environmental conditions, the horizontal size of the wave disturbance above the leading updraft cell is much smaller than that by the steady heating.

In addition to the horizontal size of the wave disturbance, the tilting slope of the phase of the wave disturbance above the leading updraft cell is shown to be larger than that by the steady heating. The tilting slope of the phase of the plane wave can be expressed by

$$\frac{z^*}{x^*} = -\frac{k^*}{m^*}, \quad (17)$$

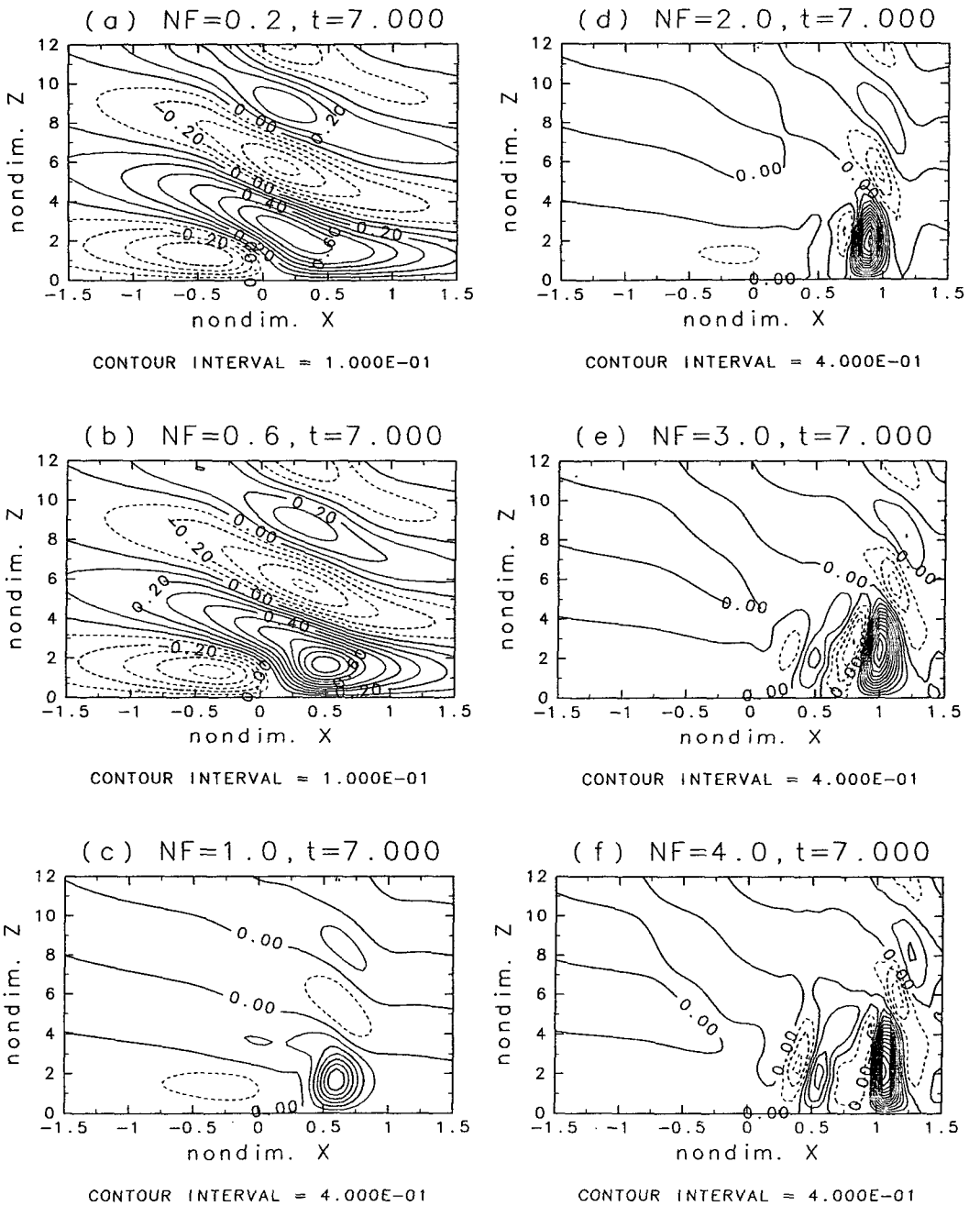

FIG. 1. The nondimensional perturbation vertical velocity fields for the nonlinearity factors of (a) 0.2, (b) 0.6, (c) 1, (d) 2, (e) 3, and (f) 4 at a time step $t = 7$. The contour intervals are 0.1 in (a) and (b) and 0.4 in (c)–(f), respectively.

where the superscript * denotes the dimensional variables and k^* and m^* are the horizontal and vertical wavenumbers, respectively. Since the vertical wavenumber (m^*) of the steady wave under the environmental conditions characterized by U and N is N/U (Smith 1979), a nondimensionalized form of (17) using the scale factors by (8) is given by

$$\frac{z}{x} = -\left(\frac{L}{L_x}\right) k, \tag{18}$$

where $k = L_x k^*$. Here, L_x is the characteristic horizontal length scale of the leading updraft cell. Note that L is the horizontal length scale of the specified steady heating, which was also used as the characteristic horizontal

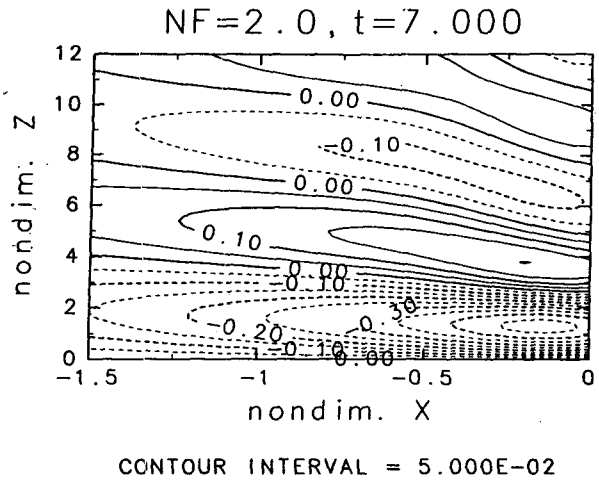

FIG. 2. As in Fig. 1d except for a portion of the domain. Contour interval of 0.05.

length scale of motion. Therefore, as long as the horizontal length scale of the leading updraft cell is smaller than that of the steady heating centered at $x = 0$, the tilting slope of the wave disturbance above the leading updraft cell is larger than that by the steady heating. From the group velocity argument, it is straightforward to show that the sign of k^*/m^* is positive (negative) for $U > 0$ ($U < 0$) for hydrostatic flow in order for wave energy to propagate upward.

Raymond (1986) showed that the phase relationship between the heating and the induced vertical velocity at the possible level of free convection depends on the inverse of the Froude number. He showed that there exist maximum positive phase relationship between the heating and the induced vertical velocity at the heating center when $\mathrm{Fr}^{-1} = 3\pi/2, 7\pi/2, 11\pi/2, \cdots$ and maximum negative phase relationship when $\mathrm{Fr}^{-1} = \pi/2, 5\pi/2, 9\pi/2, \cdots$. In our study, Fr^{-1} is equivalent to the nondimensional heating depth, which has a fixed value of 2. With $\mathrm{Fr}^{-1} = 2$, the vertical velocity and the heating has a negative phase relationship at the heating center based on Raymond's (1986) analysis.

Figure 3 shows the time-averaged maximum vertical velocity and its location from $x = 0$ as a function of the nonlinearity factor. The time average is taken over four time units from $t = 4$ to 8. The upper panel indicates that the maximum vertical velocity is almost constant up to $\mu < 0.4$, then gradually increases up to $\mu \sim 2$, and beyond this value remains little changed. It should be noted that even though the time-averaged nondimensional maximum vertical velocity is in a quasi-steady state in its magnitude for $\mu < 0.4$ and $\mu > 2$, the time-averaged dimensional maximum vertical velocity increases linearly with a linear increase of the nonlinearity factor in these ranges if the amplitude of the heating function changes linearly with the other parameters held fixed [see (8) and (16)]. The lower panel indicates that the horizontal location of the maximum vertical velocity is located farther downstream as the nonlinearity factor increases (also see Fig. 1). Although the horizontal location of the maximum vertical velocity should be, strictly speaking, on $x = 0$ for the linear case ($\mu = 0$), it is located slightly farther downstream from $x = 0$, possibly due to the numerical model truncation errors and a boundary condition problem.

Figure 4 shows the time evolution of the maximum vertical velocity for the nonlinearity factors of 0.2, 0.6, 1, 2, 3, and 4. In the case of $\mu = 0.2$, a quasi-steady state in the maximum vertical velocity is attained after $t \sim 2$ for the given damping coefficient of $\nu = 0.2$, which corresponds to an e-folding time of 5. As the nonlinearity factor further increases ($\mu = 0.6$ and 1 cases), the maximum vertical velocity gradually increases until the end of the time integration with a much greater increasing rate in the case of $\mu = 1$ than in the case of $\mu = 0.6$. The $\mu = 2$ case also exhibits a gradual increase trend in the maximum vertical velocity with time, but with a little irregular oscillatory behavior. In the $\mu = 3$ and 4 cases, the maximum vertical velocity associated with the leading updraft cell shows a regular oscillation pattern after the model is adjusted to the thermal forcing from the resting initial perturbation state. The oscillation period in the case of $\mu = 3$ (0.63) is longer than that in the case of $\mu = 4$ (0.52), and the

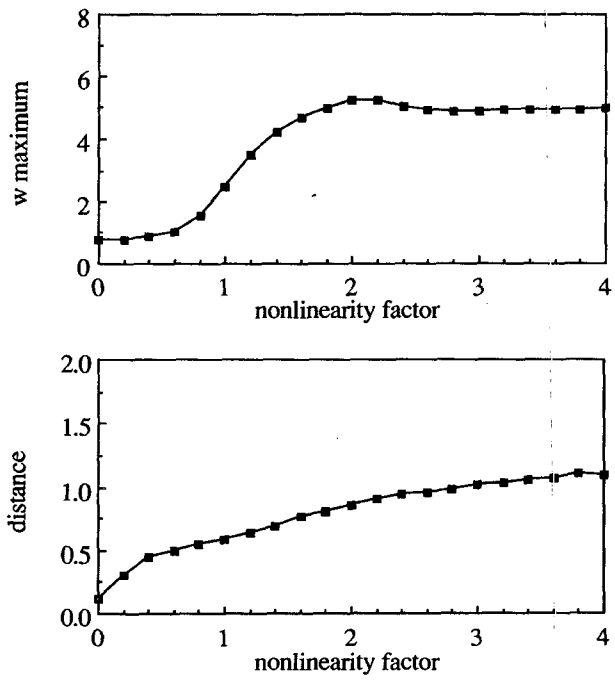

FIG. 3. The time-averaged nondimensional maximum perturbation vertical velocity (upper panel) and the time-averaged horizontal distance to the location of the nondimensional maximum perturbation vertical velocity from $x = 0$ (lower panel) as a function of the nonlinearity factor. The time average is taken from $t = 4$ to 8.

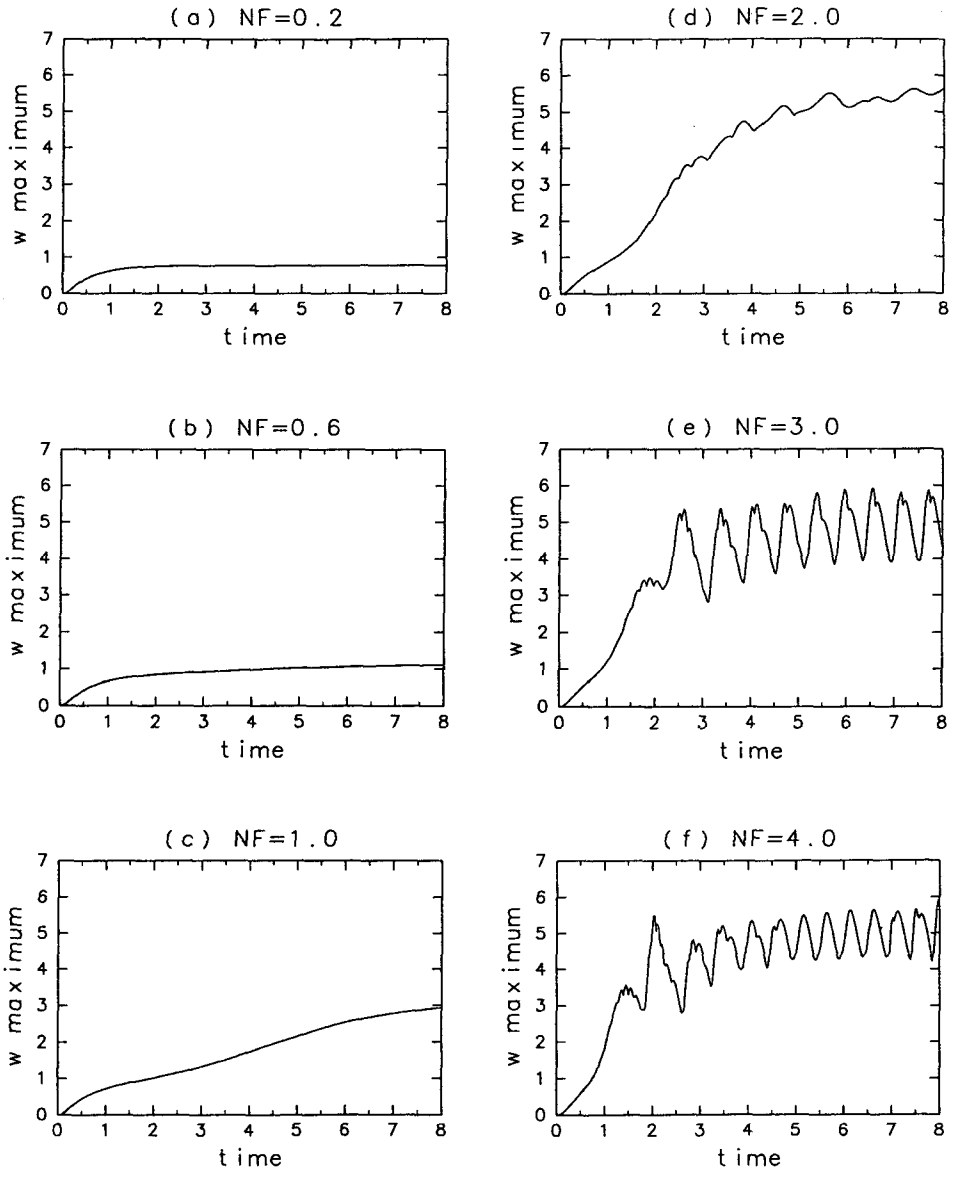

FIG. 4. The time evolution of the nondimensional maximum perturbation vertical velocity for the nonlinearity factors of (a) 0.2, (b) 0.6, (c) 1, (d) 2, (e) 3, and (f) 4.

oscillation amplitude in the former case is larger than that in the latter case.

In order to decide the critical value of the nonlinearity factor beyond which the vertical velocity undergoes a pronounced regular oscillatory behavior, we examined the time evolution of the maximum vertical velocity for the four cases that have μ values between 2 and 3. This revealed that the critical value is about 2.2. This value is close to the value beyond which the magnitude of the time-averaged maximum vertical velocity remains little changed (Fig. 3). In this study, we will use the term *highly nonlinear regime* to designate flow regime when the nonlinearity factor is $\geqslant 2.2$ for a nondimensional heating height of 2 and a performed experimental range of $0 \leqslant \mu \leqslant 4$.

Two numerical experiments with the nonlinearity factor of 3 were performed with different values of the coefficient of Rayleigh friction and Newtonian cooling ($\nu = 0.1$ and 0.3) to examine the effect of the strength of the damping coefficient on the flow field. Results showed that the flow response in these two experiments is not fundamentally different from that of the $\nu = 0.2$ case (the oscillatory behavior was also clearly observed in these two experiments), although the maximum vertical velocity decreases as the damping coefficient increases.

To investigate the effect of nonlinearity on the oscillation period, the average oscillation period in the highly nonlinear regime is plotted as a function of the nonlinearity factor in Fig. 5. This figure shows that as the nonlinearity factor increases, the oscillation period decreases (to a good approximation, the oscillation period is inversely proportional to the nonlinearity factor). This is because of the faster nonlinear advective process of the updraft and downdraft cells behind the leading updraft cell as the nonlinearity factor becomes larger.

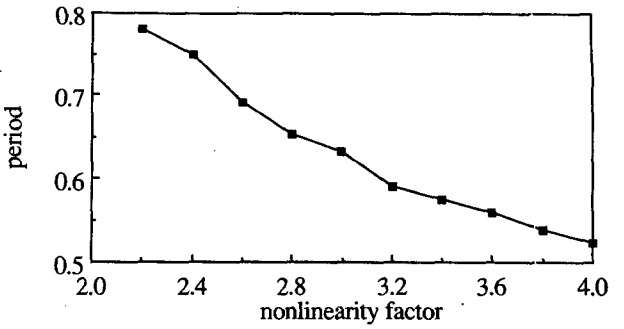

FIG. 5. The average nondimensional oscillation period as a function of the nonlinearity factor in the highly nonlinear regime.

To examine the temporal features of the updraft and downdraft cells on the downstream side, which are simulated in the highly nonlinear regime (see Figs. 1e–f), the time evolution of the vertical velocity field for the nonlinearity factor of 3 is shown in Fig. 6. The time sequence is from $t = 6.5$ to 7.125, hence spanning approximately one oscillation period (see Figs. 4e and 5). At $t = 6.5$, three successive cells behind the leading updraft cell—that is, a downdraft cell, an updraft cell and another downdraft cell (labeled by 1, 2, and 3, respectively)—are observed. At $t = 6.625$, these three cells are advected downstream, cells 2 and 3 intensify during the advective process; cell 1 is shrunk between the leading updraft cell and cell 2 and weakens. At $t = 6.75$, cell 1 shrinks further and weakens, cell 2 weakens, and cell 3 intensifies further. It is observed that the updraft cell behind cell 3 is gradually forming at $t = 6.5$ and 6.625, which is labeled by 4 at $t = 6.75$. The formation of the updraft (downdraft) cell behind cell 3 (4) is to some extent facilitated by the compensating upward (downward) motion induced by the downdraft (updraft) cell 3 (4). At $t = 6.875$, cell 1 disappears, cell 2 is about to be merged into the leading updraft cell, and cell 4 intensifies. At $t = 7$, cell 2 is already merged and the downdraft cell behind cell 4, labeled by 5, is seen to be formed. At $t = 7.125$, cells 3, 4, and 5 are advected downstream with cells 4 and 5 intensified.

This completes about one cycle of the oscillation and a similar cycle with linear and nonlinear advection, intensification, weakening, formation, disappearing, and merging processes of cells behind the leading updraft cell is repeated. The average speed of the updraft and downdraft cells behind the leading updraft cell is about 0.7. This value is larger than the vertically averaged perturbation positive horizontal velocity below the heating top height (see Fig. 9), but smaller than the total horizontal velocity in this region.

As mentioned above, Fig. 6 shows that the leading updraft cell seems to act as a stationary momentum source for the wave disturbance above it because the horizontal location of the maximum vertical velocity associated with the leading updraft cell remains little changed after $t \sim 4$ during the cycles (as shown in Fig. 7), and the averaged maximum vertical velocity for a period also does (Fig. 4e). In this context, once the magnitude of the perturbation is large enough, the wave disturbance on the downstream side is mainly controlled by the quasi-stationary leading updraft cell, even though the perturbation is initially induced by the steady heating centered at $x = 0$, which is still the only source for producing the perturbation on the upstream side.

The nonhydrostatic effect might be important as the nonlinearity factor increases, specifically in the region of the leading updraft cell. However, in this study, our concern was to study the nonlinear response of the hydrostatic atmosphere to low-level heating. Notice that the nonhydrostatic effect was ignored not by the scaling analysis, but by the hydrostatic assumption. However, further study is needed to investigate the nonhydrostatic effect on the structure of the leading updraft cell and the oscillatory behavior in the highly nonlinear flow regime.

The intensification, weakening, formation, disappearing, and merging processes of the alternating updraft and downdraft cells behind the leading updraft cell are connected with the oscillatory behavior of the perturbation horizontal velocity through the mass continuity equation for the hydrostatic, incompressible flow. Figure 8 illustrates the perturbation horizontal velocity fields corresponding to Fig. 1. As the nonlinearity factor increases, the locations of the maximum and minimum perturbation horizontal velocities are shifted farther downstream. When the nonlinearity factor becomes large enough ($\mu \geq 2.2$), the strong nonlinear advection produces the secondary maximum region of the perturbation horizontal velocity behind the primary maximum of the perturbation horizontal velocity (Figs. 8e and 8f). This existence of the secondary maximum of the perturbation horizontal velocity is believed to be a main factor in distinguishing nonlinear (highly nonlinear) response of the atmosphere to specified steady heating from the linear response.

To get some insight into the role of the secondary maximum of the perturbation horizontal velocity on the flow response, the time evolution of the perturbation horizontal velocity fields corresponding to Fig. 6 is plotted in Fig. 9. The shaded region represents the flow reversal region where the perturbation horizontal ve-

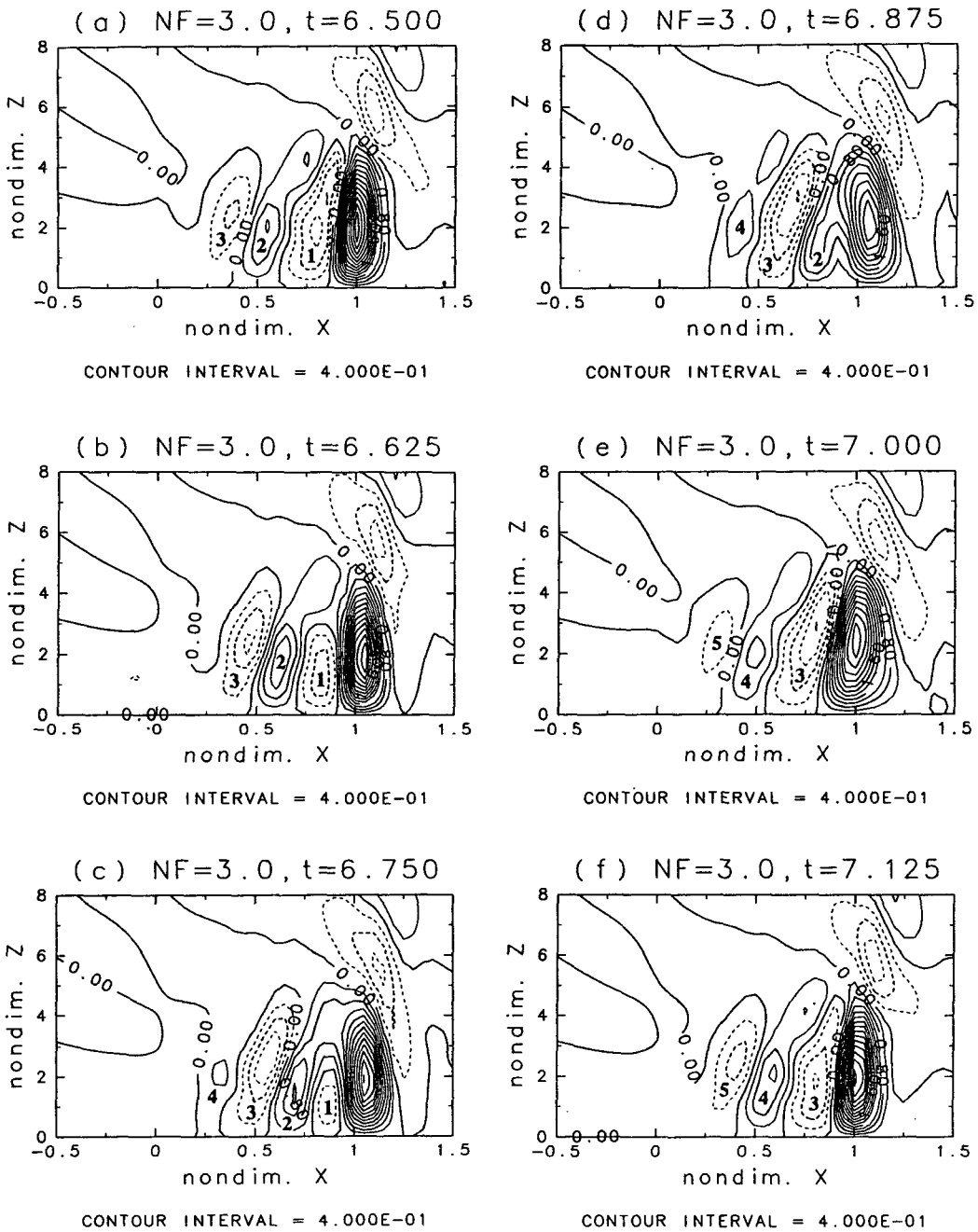

FIG. 6. The time evolution of the nondimensional perturbation vertical velocity field for the nonlinearity factor of 3 at time steps t = (a) 6.5, (b) 6.625, (c) 6.75, (d) 6.875, (e) 7, and (f) 7.125. The contour interval is 0.4, and the tick labels on the updraft and downdraft cells are explained in the text.

locity has larger magnitude than the basic-state wind with the opposite sign. From (8) and (16), it can be shown that the nondimensional total horizontal velocity is given by

$$u_T = 1 + \mu u. \tag{19}$$

Therefore, the total flow is reversed against the basic-state flow direction when $u < -1/\mu$.

At $t = 6.5$, the primary maximum of the perturbation horizontal velocity is located near $x = 0.85$ at the surface and the secondary maximum of the perturbation horizontal velocity near $x = 0.39$. At $t = 6.625$, the

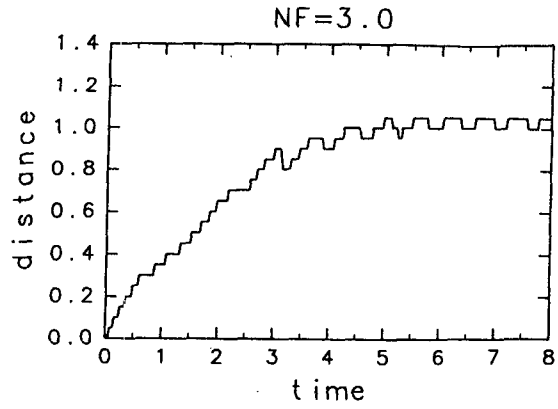

FIG. 7. The time evolution of the horizontal location of the nondimensional maximum perturbation vertical velocity from $x = 0$ for the nonlinearity factor of 3.

primary maximum weakens and the secondary maximum intensifies. At $t = 6.75$, the secondary maximum becomes a new primary maximum, while the previous primary maximum begins to disappear. Note that the vertical velocity of the leading updraft cell is still much stronger than that of cell 2 (see Fig. 6) even when the secondary maximum becomes the primary maximum. This is because the vertical velocity is related to the horizontal gradient of the perturbation horizontal velocity rather than the perturbation horizontal velocity itself. However, the vertical velocity of the leading updraft cell indeed decreases when the secondary maximum becomes the primary maximum. At $t = 6.875$, the secondary maximum has already disappeared, the new primary maximum is shifted downstream and a new secondary maximum appears near $x = 0.25$. The secondary maximum intensifies at $t = 7$ corresponding to the time of the completion of the merging of cell 2 into the leading updraft cell (see Figs. 6d and 6e). At $t = 7.125$, the secondary maximum further strengthens its intensity and the situation is very similar to that at $t = 6.5$. And, a similar cycle is repeated again for the oscillation period.

The above process is connected with the periodic oscillatory behavior of the vertical velocity as shown in Figs. 4e (also 4f) and 6. The above process can explain the steadiness of the time-averaged maximum vertical velocity for an oscillation period associated with the leading updraft cell in spite of the continuous supply of the heating centered at $x = 0$. This is possible because the nonlinear advection prevents the maximum perturbation from continuously strengthening its intensity by producing the secondary maximum of the perturbation horizontal velocity, which during its downstream advection intensifies and causes the primary maximum of the perturbation horizontal velocity to diminish and becomes a new primary maximum for an oscillation period. As the nonlinearity factor becomes larger, the process described in Fig. 9 takes place faster and the oscillation period becomes shorter (Fig. 5).

To examine whether the horizontal structure of the specified heating affects the existence of the secondary maximum of the perturbation horizontal velocity, an experiment was performed in which all the parameters are the same as those in the $\mu = 3$ case except that the horizontal heating structure is uniformly specified in such a way that $f(x) = 1$ for $-0.5 \leq x \leq 0.5$ and $f(x) = 0$ otherwise [see (14)]. The periodic oscillatory behavior described above was also observed in this experiment (not shown here). Therefore, it appears that the periodic oscillatory behavior in the highly nonlinear, two-dimensional, hydrostatic flow with a specified heating is an inherent response regardless of, at least, the horizontal structure of the heating.

Figure 9 shows that the location of the minimum perturbation horizontal velocity located between $z = 3$ and 4 is in phase with that of the maximum perturbation horizontal velocity; that is, the shaded region is located just above the region of the primary maximum of the perturbation horizontal velocity. Since the shaded region is the region of the maximum nonlinear effect in the region of the negative perturbation horizontal velocity, the horizontal movement of the location of the maximum or minimum perturbation horizontal velocity represents that of the maximum nonlinear effect. The periodic oscillatory change of the minimum perturbation horizontal velocity can be explained by the process similar to that for the maximum perturbation horizontal velocity described above.

Using the perturbation method, Chun and Baik (1994) solved a weakly nonlinear problem for the two-dimensional, steady-state, inviscid airflow system in a uniform basic-state flow with diabatic forcing. They found that the main weakly nonlinear effect is that cooling, which is induced by the specified diabatic heating, produces convergence near the surface, hence resulting in upward motion in the center of the forcing region that extends upstream. Based on this result, they speculated that in the steady-state problem as the nonlinearity increases, the first-order upward motion may overcome the zeroth-order downward motion near the heating center. However, in the time-dependent problem in the highly nonlinear regime, Figs. 1 and 6 reveal that there is always downward motion near the heating region and quasi-steady-state field cannot be achieved. Therefore, as somewhat expected in the highly nonlinear regime, a fundamental dynamical difference between a steady-state problem and a time-dependent problem exits. It would be of great value in digging out the nature of nonlinearity to solve a steady-state, fully nonlinear problem and compare its results with a time-dependent nonlinear numerical solution. This problem remains highly challenging.

Nonlinear response of a stably stratified uniform flow to steady heat source for different nonlinearity factors can be clearly seen from the streamfunction fields.

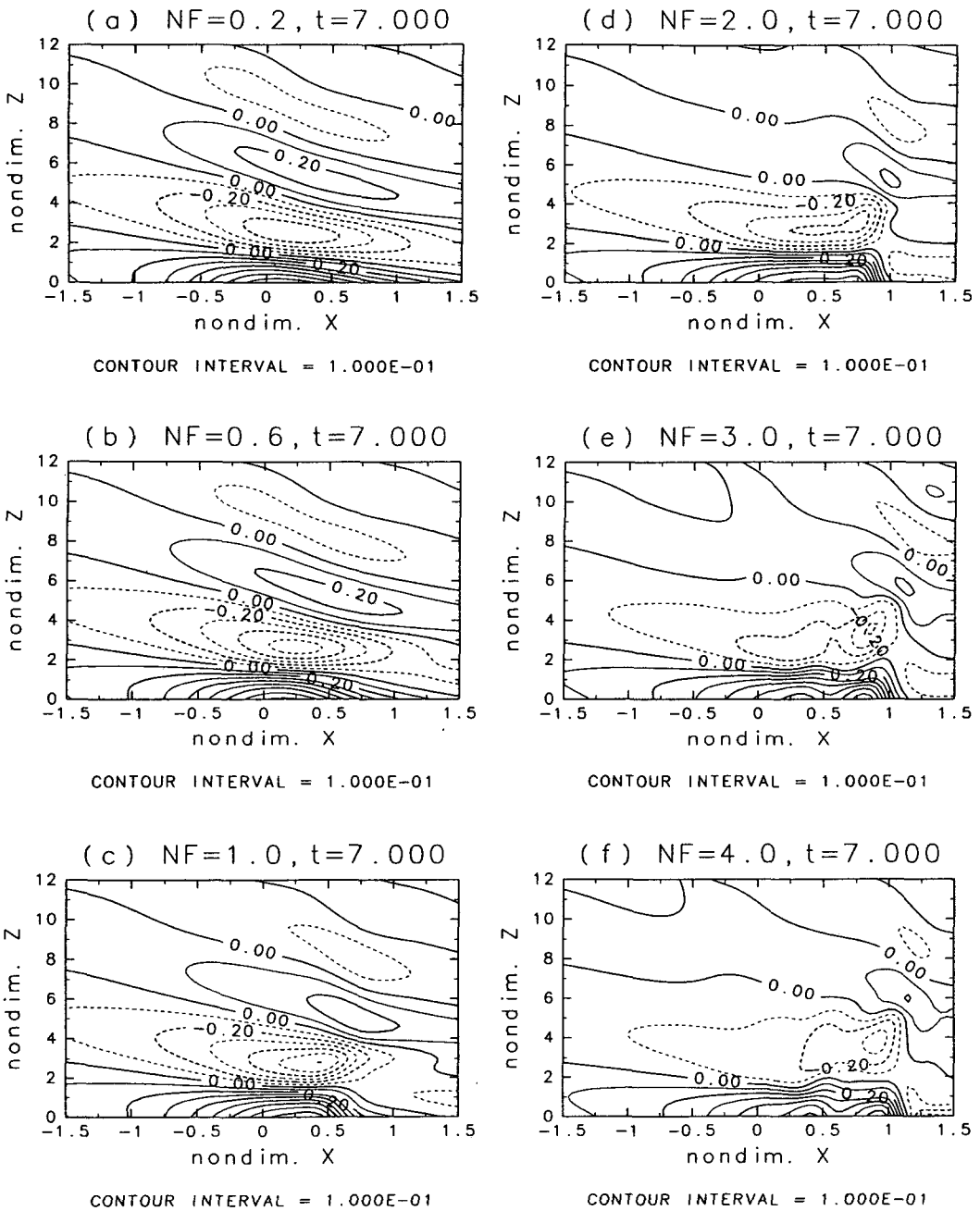

FIG. 8. The same as in Fig. 1 except for the nondimensional perturbation horizontal velocity field. The contour interval is 0.1.

From (11), the nondimensional perturbation streamfunction φ can be defined as

$$\frac{\partial \varphi}{\partial x} = -w, \quad \frac{\partial \varphi}{\partial z} = u. \tag{20}$$

Then, the nondimensional total streamfunction φ_T for the uniform flow can be obtained by

$$\varphi_T = z + \mu \int_0^z u dz. \tag{21}$$

Figure 10 shows the total streamfunction fields for the nonlinearity factors of 0.6 (Fig. 10a) and 3 (Fig. 10b) at a time step $t = 7$. In the case of $\mu = 0.6$, the total streamfunction resembles the steady state linear solution. On the other hand, the total streamfunction field

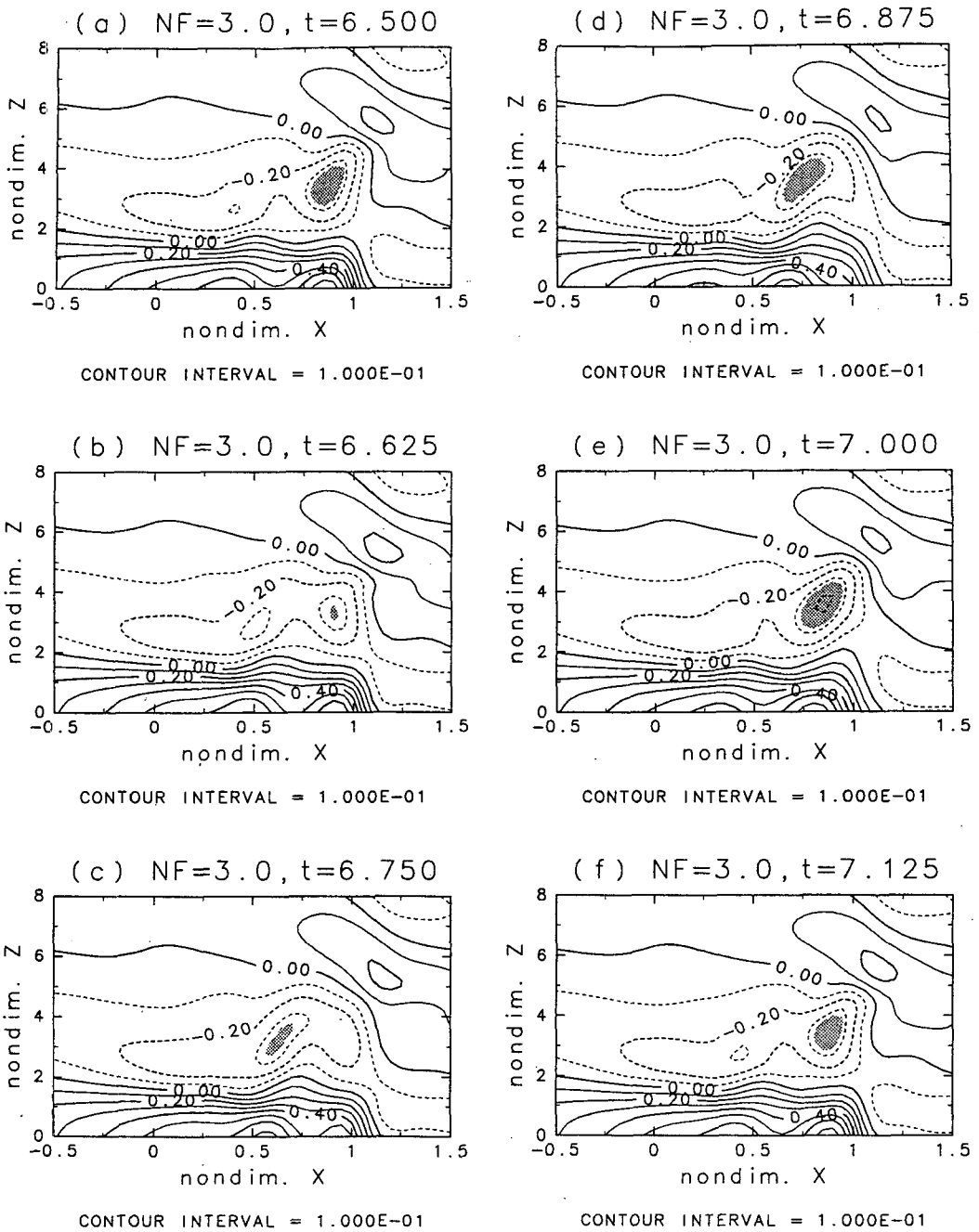

FIG. 9. The same as in Fig. 6 except for the nondimensional perturbation horizontal velocity field. The contour interval is 0.1 and the regions of $u < -1/3$ are shaded.

for the strong nonlinearity case (Fig. 10b) is quite different from that in Fig. 10a. The flow response near $z = 2$ to 4 is related to the negative perturbation horizontal velocity near that region as shown in Fig. 8e. According to the linear theory for the response of a stably stratified uniform flow to steady heating, the maximum perturbation horizontal velocities exist at the heights of $z^* = 2n\pi/\lambda^*$, $n = 0, 1, 2, 3, \cdots$, and the minimum perturbation horizontal velocities exist at the heights of $z^* = (2n + 1)\pi/\lambda^*$, $n = 0, 1, 2, 3, \cdots$ (Chun 1991). Here, the superscript * denotes the dimensional variables and $\lambda^* = N/U$. Note that there is a $\pi/4$ phase difference in the heights for the maximum or minimum perturbation horizontal velocities between thermally induced waves and mechanically induced mountain waves. When the characteristic scales introduced in (8)

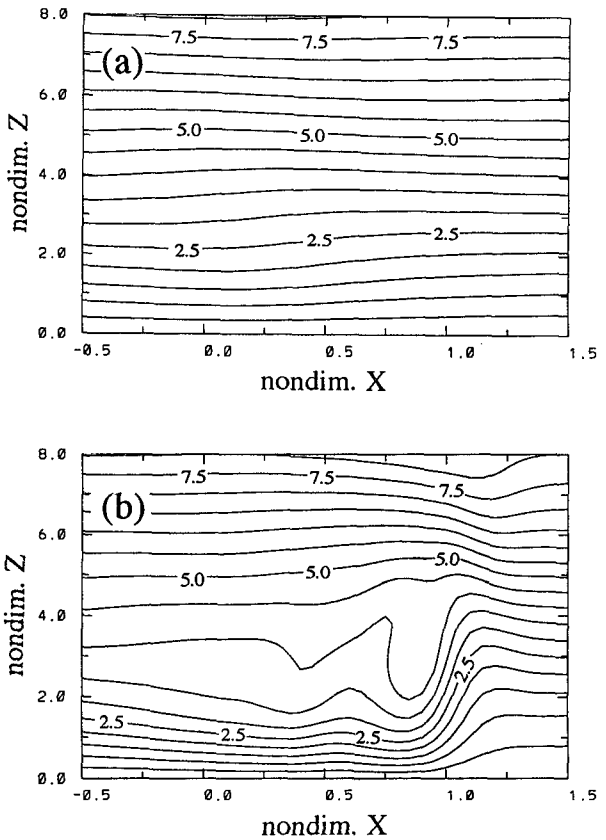

FIG. 10. The nondimensional total streamfunction fields for the nonlinearity factors of (a) 0.6 and (b) 3 at a time step $t = 7$. The contour interval is 0.5.

are used, the nondimensional heights for the maximum and minimum perturbation horizontal velocities are $z = 2n\pi$ and $z = (2n + 1)\pi$, respectively.

In fact, the minimum perturbation horizontal velocity of about -0.4 near $z = \pi$ makes the total horizontal velocity be small negative there (see Fig. 9e). This implies that there may exist a local wave breaking. The mixing related to the wave breaking is well represented by the total streamfunction near $z = 2$ to 4 and $x = 0.75$ to 1. The location of the wave-induced critical level (Clark and Peltier 1984) is well matched with the wave steepening height of the linear theory (Chun 1991). Once a wave-induced critical level exists, the wave induced by low-level heating may be reflected from the critical level and the wave amplification in the lower layer is possible. Even though the large value of the nonlinearity factor itself amplifies the dimensional perturbation horizontal velocity both near the surface and wave steepening height, the possible local wave reflection from the self-induced critical level may even enhance the wave amplitude in the lower layer.

As discussed in Durran (1986), we may analogize this case (Fig. 10b) to hydraulic theory through the local wave breaking. A self-induced critical level may provide the effective upper boundary condition, which can constrain the modal structure of gravity waves in the lower layer between the critical level and the surface. In other words, flow might be supercritical with respect to these modes even though infinitely deep, continuously stratified flow cannot be supercritical with respect to vertically propagating waves. Therefore, the flow could undergo a transition from subcritical upstream to supercritical flow downstream.

In the application of nonlinear response of a stably stratified atmosphere to low-level heating to hydraulic theory, there appears to be some problems. Besides the fundamental differences between our infinitely deep, continuously stratified atmosphere and shallow water system, there is a difference between thermally induced waves and mechanically induced waves. For thermally induced waves, surface drag should be zero no matter how large the perturbation horizontal velocity at the surface is because of the flat bottom lower boundary condition (Chun 1991). Since the lower boundary condition provides the source of wave energy for mountain waves, the wave energy generation and the energy exchange between the atmosphere and the surface might be different in these two cases. It seems that we need more systematic numerical experiments for analogy of our strong nonlinear case to hydraulic theory, even though the total streamfunction field looks like a hydraulic-like jump.

4. Summary and conclusions

Effects of nonlinearity on the stably stratified atmospheric response to prescribed low-level heating were investigated by performing nondimensional numerical model experiments over a wide range of the nonlinearity factors of thermally induced waves ($0 \leq \mu \leq 4$). The airflow system considered was a two-dimensional, hydrostatic, nonrotating, Boussinesq system with a constant stability and a uniform basic-state horizontal wind. The diabatic heating was specified to be uniform in the vertical from the surface to a nondimensional height of 2 and bell shaped in the horizontal.

It was shown that as the nonlinearity factor increases, the flow response becomes quite different from the linear response because of the increasing nonlinear advective effect. On the downstream side, a strong updraft cell gradually appeared with increasing nonlinearity factor. In the highly nonlinear regime ($\mu \geq 2.2$), alternating weaker downdraft and updraft cells behind the leading updraft cell were simulated on the downstream side. The perturbation flow analysis indicated that these alternating cells experience periodic cycles with the processes of linear and nonlinear advection, intensification, weakening, formation, disappearing, and merging to the leading updraft cell. It was found that as the nonlinearity factor increases, the oscillation period in the maximum vertical velocity associated

with the leading updraft cell decreases. The horizontal location of the maximum vertical velocity was shown to be located farther downstream as the nonlinearity factor increases. However, regardless of μ values, there existed a negative phase relationship between the heating and the induced vertical displacement in the vicinity of the heat source and the gravity wave response characteristics on the upstream side.

In fact, the vertical velocity was diagnostically determined by the perturbation horizontal velocity through the mass continuity equation for the hydrostatic, incompressible flow. Therefore, the intensification, weakening, formation, disappearing, and merging processes of the alternating updraft and downdraft cells behind the leading updraft cell are connected with the oscillatory behavior of the perturbation horizontal velocity for a period. In the highly nonlinear regime, there existed the secondary maximum of the perturbation horizontal velocity behind the primary maximum of the perturbation horizontal velocity at the surface. During its downstream advection, this secondary maximum intensified, caused the primary maximum ahead to diminish, and became a new primary maximum for an oscillation period. It was suggested that this oscillatory behavior (occurring faster for the larger nonlinearity factor) and the steadiness of the maximum perturbation averaged over a period are main features of the nonlinear response of the two-dimensional, hydrostatic atmosphere to specified steady heating. These are clearly distinguishable from the weakly nonlinear steady-state response of the atmosphere to specified steady heating by Chun and Baik (1994).

For the strong nonlinear case, the location of the wave-induced critical level was well matched with the wave steepening height of the linear theory. It was speculated that even though the large value of nonlinearity factor itself amplifies the dimensional perturbation horizontal velocity both near the surface and wave steepening height, the possible local wave reflection from the self-induced critical level may even enhance the wave amplitude in the lower layer.

It has been recognized that the vertical extent of thermal forcing has a significant influence on the induced circulations. To test how flow regimes change with changing nondimensional heating depth (d) or the inverse Froude number associated with the thermal forcing, we performed some numerical experiments in which d varies with some fixed values of μ. Except for d and μ values, other parameters were kept the same as the previous experiments. Let us take three examples briefly. In an experiment with $d = 1$ and $\mu = 1$, an updraft cell on the downstream side continued to move downstream with gradually weakening strength at later time steps and alternating updraft and downdraft cells behind it were not observed (cf. with the case with $d = 2$ and $\mu = 1$ in Fig. 1c). In an experiment with $d = 3$ and $\mu = 3$, a strong updraft cell near $x = 0$ was predominant and was almost stationary (cf. with the case with $d = 2$ and $\mu = 3$ in Fig. 1e). However, when d was increased to 4 with $\mu = 3$, the qualitative flow response was similar, but the updraft cell was weaker compared with the case with $d = 3$ and $\mu = 3$. These latter two examples imply that the maximum magnitude of the vertical velocity appears to depend upon the nondimensional heating depth as in the weakly nonlinear steady-state case by Chun and Baik (1994) [see Fig. 8 of their paper].

The above examples indicate that the flow response is indeed sensitive to the nondimensional heating depth or the inverse Froude number associated with thermal forcing. In this study, we focused on the nonlinear effects by varying the nonlinearity factor but fixing the nondimensional heating depth. Since the flow regime drastically changes with changing d as well as μ, a systematic and extensive numerical study is needed in the μ–d parameter space to further extend the present flow response regime and advance our understanding of the nonlinear nature of a flow system. Also, in this study, we considered the vertical heating structure that extended from the surface to a certain height for a simplicity. A further study for an elevated heating is necessary to examine what mechanism in the nonlinear regime produces, if any, possible differences in the flow response fields between the present heating profile and an elevated heating. These two problems deserve further investigation.

Acknowledgments. Part of this research was performed while the first author was at the Center for Climate System Research, University of Tokyo as visiting associate professor. He would like to thank the University of Tokyo for providing his associate professorship and Prof. Taroh Matsuno and Prof. Masaaki Takahashi for their sincere support during his stay. The authors would like to thank reviewers for providing valuable comments on this study. The first author was supported by the research fund given to Kwangju Institute of Science and Technology by the Korea Ministry of Science and Technology.

REFERENCES

Adomian, G., 1994: *Solving Frontier Problems of Physics: The Decomposition Method.* Kluwer Academic Publishers, 352 pp.

Asselin, R., 1972: Frequency filter for time integrations. *Mon. Wea. Rev.*, **100,** 487–490.

Baik, J.-J., 1992: Response of a stably stratified atmosphere to low-level heating—An application to the heat island problem. *J. Appl. Meteor.*, **31,** 291–303.

Barcilon, A., J. C. Jusem, and S. Blumsack, 1980: Pseudo-adiabatic flow over a two-dimensional ridge. *Geophys. Astrophys. Fluid Dyn.*, **16,** 19–33.

Bretherton, C., 1988: Group velocity and the linear response of stratified fluids to internal heat or mass sources. *J. Atmos. Sci.*, **45,** 81–93.

Chun, H.-Y., 1991: Role of a critical level in a shear flow with diabatic forcing. Ph.D. dissertation, North Carolina State University, 159 pp.

——, and J.-J. Baik, 1994: Weakly nonlinear response of a stably stratified atmosphere to diabatic forcing in a uniform flow. *J. Atmos. Sci.*, **51,** 3109–3121.

Clark, T. L., and W. R. Peltier, 1984: Critical level reflection and the resonant growth of nonlinear mountain waves. *J. Atmos. Sci.*, **41,** 3122–3134.

Durran, D. R., 1986: Another look at downslope windstorms. Part I: The development of analogs to supercritical flow in an infinitely deep, continuously stratified fluid. *J. Atmos. Sci.*, **43,** 2527–2543.

Fraser, A. B., R. Easter, and P. Hobbs, 1973: A theoretical study of the flow of air and fallout of solid precipitation over mountainous terrain. *J. Atmos. Sci.*, **30,** 813–823.

Klemp, J. B., and D. R. Durran, 1983: An upper boundary condition permitting internal gravity wave radiation in numerical mesoscale models. *Mon. Wea. Rev.*, **111,** 430–444.

Lin, C. A., and R. E. Stewart, 1991: Diabatically forced mesoscale circulations in the atmosphere. *Adv. Geophysics,* Vol. 33, Academic Press, 267–305.

Lin, Y.-L., 1994: Airflow over mesoscale heat sources. Part I: Responses in a uniform flow. *Proc. Nat. Sci. Counc. ROC(A),* **18,** 1–32.

——, and R. B. Smith, 1986: Transient dynamics of air flow near a local heat source. *J. Atmos. Sci.*, **43,** 40–49.

——, and R. C. Goff, 1988: A study of a mesoscale solitary wave in the atmosphere originating near a region of deep convection. *J. Atmos. Sci.*, **45,** 194–205.

——, and H.-Y. Chun, 1991: Effects of diabatic cooling in a shear flow with a critical level. *J. Atmos. Sci.*, **48,** 2476–2491.

Navon, I. M., and H. A. Riphagen, 1979: An implicit compact fourth-order algorithm for solving the shallow-water equations in conservation-law form. *Mon. Wea. Rev.*, **107,** 1107–1127.

Olfe, D. B., and R. L. Lee, 1971: Linearized calculations of urban heat island convection effects. *J. Atmos. Sci.*, **28,** 1374–1388.

Orlanski, I., 1976: A simple boundary condition for unbounded hyperbolic flows. *J. Comput. Phys.*, **21,** 251–269.

Perkey, D. J., 1976: A description and preliminary results from a fine-mesh model for forecasting quantitative precipitation. *Mon. Wea. Rev.*, **104,** 1513–1526.

Raymond, D. J., 1986: Prescribed heating of a stratified atmosphere as a model for moist convection. *J. Atmos. Sci.*, **43,** 1101–1111.

Smith, R. B., 1979: The influence of mountains on the atmosphere. *Adv. Geophysics,* Vol. 21, Academic Press, 87–230.

——, and Y.-L. Lin, 1982: The addition of heat to a stratified airstream with application to the dynamics of orographic rain. *Quart. J. Roy. Meteor. Soc.*, **108,** 353–378.

Thorpe, A. J., M. J. Miller, and M. W. Moncrieff, 1980: Dynamical models of two-dimensional downdraughts. *Quart. J. Roy. Meteor. Soc.*, **106,** 463–484.